Influence of the electrode-electrolyte interface on electrochemical CO2 reduction reaction and hydrogen evolution reaction

Ye, C.

Chapter 2

Enhanced Electrochemical CO_2 Reduction to Formate on Poly(4-vinylpyridine)-modified Copper and Gold Electrodes

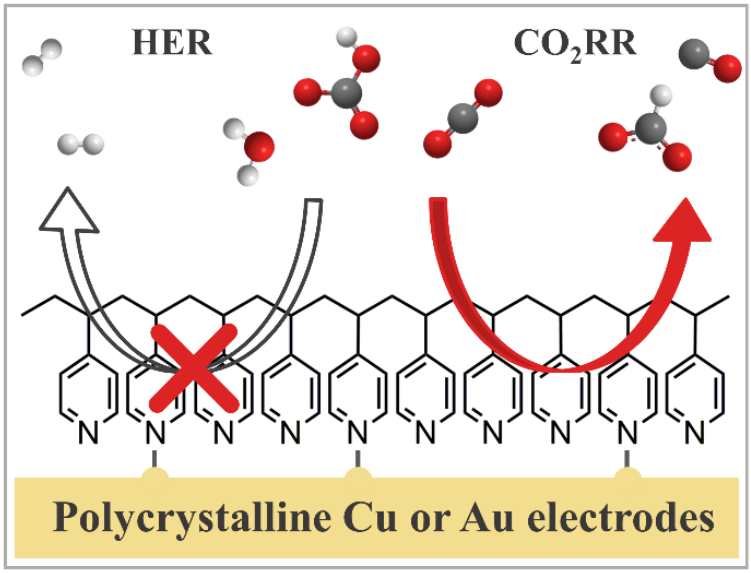

This chapter is based on:

Ye, C.; Raaijman, S. J.; Chen, X.; Koper, M. T. M. *ACS Appl. Mater. Interfaces* **2022,** *14* (40), 45263-45271

Abstract: Developing active and selective catalysts converting CO_2 to valuable products remains a critical challenge for further application of the electrochemical CO_2 reduction reaction (CO_2RR). Catalytic tuning with organic additives/films has emerged as a promising strategy to tune CO_2RR activity and selectivity. Herein we report a facile method to significantly change CO_2RR selectivity and activity of copper and gold electrodes. We found improved selectivity towards HCOOH at low overpotentials on both polycrystalline Cu and Au electrodes after chemical modification with a poly (4-vinylpyridine) (P4VP) layer. In situ ATR-SEIRAS and contact angle measurements indicate that the hydrophobic nature of the P4VP layer limits mass transport of HCO_3^- and H_2O, whereas it has little influence on CO_2 mass transport. Moreover, the early onset of HCOOH formation and the enhanced formation of HCOOH over CO suggests that P4VP modification promotes a surface hydride mechanism for HCOOH formation on both electrodes.

2.1 Introduction

The electrochemical CO_2 reduction reaction (CO_2RR) provides a promising route to utilize carbon feedstock and store renewable electrical energy. Various products, such as formic acid, carbon monoxide, hydrocarbons and alcohols, can be obtained via the CO_2RR in aqueous media. Extensive experimental and theoretical work has been dedicated to investigate the CO_2RR process to different products.[1-4] The initial two-electron transfer products formed during the CO_2RR in aqueous media are formic acid (HCOOH) and carbon monoxide (CO), with subsequent further reduced products commonly agreed upon as resulting from CO reduction (mainly on copper (Cu) catalysts).[5] Due to the high ratio of molecular weight per electron transferred, formic acid has been considered one of the most economically interesting products.[6-7] However, HCOOH-selective catalysts such as Sn, Pb and Pd either require high overpotentials (>0.8 V) or suffer from low stability,[8-10] which limits their application. Therefore, discovering the factors which govern the selectivity of CO_2RR to HCOOH could open up the possibility of selective HCOOH synthesis from CO_2RR with higher efficiency.

Despite extensive efforts of the scientific community, achieving high selectivity at low overpotentials remains a significant challenge for the CO_2RR.[11-14] One strategy to influence product selectivity is catalyst modification with organic additives such as poly (4-vinyl pyridine) (P4VP),[15] N-substituted pyridinium,[16] poly(acrylamide) (PAM),[17] and N,N'-ethylene-phenanthrolinium dibromide[18]. Coating polycrystalline Cu electrodes with P4VP yields improved formic acid selectivity with maximum faradaic efficiency (FE) of ca. 40%.[15] Polycrystalline Cu electrodes modified with N-substituted pyridinium additives instead produce C_2 and C_3 products with total FE of ca. 70-80% (although these electrodes also show enhanced formic acid formation at low overpotential).[16] Cu surface modification by polyaniline results in similar behavior, improving selectivity towards C_{2+} hydrocarbons to ca. 80%.[19] There are two main considerations explaining how additives affect the activity and selectivity of CO_2RR catalysts: i) by influencing the catalytic activity (by stabilizing/destabilizing reaction intermediates) and/or ii) by changing the local concentration

of interfacial species involved in the reaction.[20-21] To illustrate, a higher CO coverage on polyaniline coated polycrystalline Cu catalysts,[19] an increased local pH for polycrystalline Cu electrodes modified with N-substituted pyridinium additives[16], and enhanced stabilization of the CO dimer on PAM modified Cu polycrystalline catalysts[17] have been speculated to increase the selectivity towards C_{2+} hydrocarbons, whereas the unfavorable H_2O dissociation and limited mass transport of proton donors (H_2O and HCO_3^-) have been proposed to lead to the suppression of the hydrogen evolution reaction (HER) on alkanethiol modified Cu mesh electrodes[22] and cetalkonium chloride modified polycrystalline Sn eletrodes[23]. Furthermore, recent computational studies have demonstrated a relation between changes in hydrophobicity resulting from functionalization of a Cu surface with organic molecules, and the tendency to form surface hydrides.[24] In the latter work, it was proposed that hydrophilic interfaces promote the formation of surface hydrides, which enhance the formation of formic acid, while hydrophobic interfaces favor CO formation instead.[24] These proposed explanations on the role of additives were mainly focused on multi-carbon products. More experimental evidence to elucidate the enhanced HCOOH formation is still highly desirable.

To investigate to what extent organic additives affect CO_2RR activity and selectivity, we studied the CO_2RR on polycrystalline Cu (poly Cu) and Au (poly Au) electrodes with and without P4VP layer coating, focusing on changes in the catalytic activity and product distribution. In agreement with the literature,[15] we observe an increase in selectivity of CO_2RR to HCOOH on a P4VP modified polycrystalline Cu (P4VP-modified Cu) electrode. Interestingly, this same effect is also observed on a P4VP-modified polycrystalline Au (P4VP-modified Au) electrode, even though pristine Au is a highly selective catalyst for reducing CO_2 to CO.[25-26] Our results suggest that surface modification with a P4VP layer results in enhanced selectivity towards HCOOH during the CO_2RR, regardless of the nature of electrocatalysts. To better understand this behavior, we employed in situ Attenuated Total Reflection Surface-Enhanced Infrared Reflection-Adsorption Spectroscopy (ATR-SEIRAS) to investigate the interfacial reaction species during the CO_2RR on P4VP-modified electrodes. We show that, apart from the interaction between the P4VP layer and the metal catalysts influencing catalysis, organic layer-induced limitations in mass transport of H_2O and HCO_3^-

result in a local environment rich in CO_2, which thereby increases CO_2RR rate whilst suppressing the HER. Finally, the selective enhancement of HCOOH formation over CO at low overpotentials suggest a surface hydride pathway to HCOOH. Our work thereby offers a more comprehensive understanding of the role of P4VP layer in tuning CO_2RR activity and selectivity.

2.2 Experimental Section

Cleaning. Milli-Q water (resistivity > 18.2 MΩ·cm, TOC < 5 ppb) was used for all experiments in this work. Prior to each experiment, all cell compartments were cleaned by soaking in an aqueous solution of 1 $g \cdot L^{-1}$ $KMnO_4$ (Fluka, ACS reagent) and 0.5 M H_2SO_4 (Fluka, ACS reagent) overnight. The solution was subsequently drained and the cell compartments were rinsed with a dilute piranha solution (1:3 v/v of H_2O_2 (Merck, Emprove exp) / H_2SO_4) to remove residual $KMnO_4$ and MnOx. Afterwards, the cell compartments were cleaned by repetitively rinsing and boiling with Milli-Q water to remove all inorganic contaminants.

Electrode preparation. A polycrystalline Cu disk electrode (Mateck, 99.995%), a polycrystalline Au disk electrode (Mateck, 99.95%) and a pyrolytic graphite disk electrode (PY001009, Graphite Store) were used as working electrodes. Prior to each experiment, working electrodes were mechanically polished with a diamond suspension (MetaDi, 0.5 μm, Buehler) on a microcloth (Buehler), followed by rinsing with Milli-Q water to remove residual diamond suspension. Afterwards, polycrystalline copper and polycrystalline gold electrodes were electropolished as per the following procedures. Polycrystalline copper electrodes were electropolished in a 10:5:2 solution of H_3PO_4 (Merck, 85%): H_2O: H_2SO_4 (Fluka, ACS Reagent) at +3 V vs a graphite electrode for 30 s. Polycrystalline Au electrodes were first oxidized in 0.1 M H_2SO_4 at +10 V vs the graphite electrode for 20 s and then dipped into 6 M HCl (Merck, ACS reagent, 37%) for 30 s to remove the oxide layer. The obtained eletropolished electrodes were further rinsed with Milli-Q water and dried under compressed air flow. P4VP-modified electrodes were obtained by dropcasting 10 μL of 100 mg mL^{-1} P4VP (Aldrich, Mw~60000) in dichloromethane (Actu-all chemicals) solution on

dried polycrystalline Cu and Au disk electrodes, and drying the electrodes in air for 30 minutes until all dichloromethane had evaporated.

Surface characterization. All AFM imaging was carried out in air with a JPK NanoWizard 3. A SNL (Bruker, resonance frequency: 65 kHz, spring constant: 0.35 N/m) tip was used. The AFM scan rate was 1 Hz, and the images were taken in tapping mode. All the contact angle measurements were carried out with a contact angle goniometer (Ramé-hart, model 250): 3 μL of Milli-Q H_2O was dropped onto the electrode, and the images were taken within 5 s after H_2O was dropped on the electrodes. The contact angle measurements were performed three times to confirm the trend, all electrodes were freshly prepared each time.

Electrochemistry. All electrochemical experiments were carried out in a H-type electrochemical cell equipped with three electrodes. The cathode and anode were separated by Nafion 117 membrane (Aldrich, thickness: 0.0006 inch). A dimensionally stable anode (Magneto Special Anodes) was used as a counter electrode, and a leakless Ag/AgCl (EDAQ) was used as a reference electrode. All reported potentials were converted to the reversible hydrogen electrode (RHE) scale. All working potentials were controlled with a Bio-logic SP-300 Potentiostat under room temperature. The working electrolyte was an aqueous 0.1 M $KHCO_3$ solution, made from Milli-Q water and $KHCO_3$ (Fluka, ACS reagent). Before every CO_2 reduction experiment, CO_2 (Linde, 4.5) was bubbled through the electrolyte for 30 minutes to obtain a CO_2 saturated solution. Blank cyclic voltammograms were first taken to characterize the surface and to stabilize the initial state of the electrode. The ohmic resistance was evaluated by electrochemical impedance spectroscopy (EIS) at 0.1 V vs RHE, and 85% ohmic drop compensation was applied to all subsequent experiments. Electrolysis was performed at fixed potentials for 30 minutes, constantly purging the electrolyte at 8 mL/min CO_2 for a stable pH and continuous CO_2 supply. Gas and liquid samples were taken every 10 minutes. After all experiments, P4VP layer remains intact on both poly Cu and Au electrodes under our working conditions, as evidenced by the cyclic voltammograms of P4VP-modified electrodes after CO_2RR in Figure A.6.

The gas products from CO_2 reduction were analyzed by a GC-2010 plus system (Shimadzu). The GC system was equipped with two columns. A RTX-1 column (Restek) connected to a FID was used to separate and detect hydrocarbons (CH_4, C_2H_4), and a ShinCarbon ST micropacked 80/100 column (Restek) connected to a TCD was used for H_2 and CO. Liquid products were analyzed via HPLC with an Aminex HPX-87H column (BioRad) equipped with a RID detector (Shimadzu). The detection limit for H_2, CO and HCOOH was 75 ppm, 10 ppm and 0.1 mM, respectively. Due to low production at low overpotentials and the detection limit of GC and HPLC, experiments were performed three times to ensure the experimental reproducibility. Total FEs of all products with error bars are around 100% at all electrodes, without further normalization.

In situ ATR-SEIRAS. A thin layer of poly Cu or Au (ca. 70 nm thickness) was deposited on either a silicon (for Cu) or ZnSe (for Au) prism via magnetron sputtering machine (Leybold, Z-400). The obtained Cu and Au films were used as working electrode during in situ ATR-SEIRAS experiments with an IR spectrometer (Bruker, Vertex 80v). To avoid H_2O formation from HCO_3^-, 0.1M $KDCO_3$ solution was prepared by dissolving 0.05 M K_2CO_3 in D_2O and subsequent saturation with CO_2, which was then used as working electrolyte in all experiments in D_2O solutions. The background spectra were taken at open circuit potential in H_2O or D_2O (sigma, 99.9 atom % D) before each experiment. Afterwards, the working electrolyte was added to the cell. Before CO_2 reduction experiments, cyclic voltammograms were taken in CO_2 saturated solutions to initialize the surface until the spectrum was stable. After that, the sample spectra were taken during LSV from 0.3 V vs RHE to target negative potentials on different working electrode at 1 mV s^{-1}. All spectra were taken in absorbance mode by averaging over 200 scans with a 4 cm^{-1} resolution.

2.3 Results and Discussion

Cyclic voltammetry in aqueous CO_2-saturated 0.1 M $KHCO_3$ was used to characterize the initial state of the electrodes. Figure 2.1a shows the cyclic voltammograms of the unmodified poly Cu (black curve) and the P4VP-modified Cu electrodes (red curve), respectively. The poly Cu electrode shows a cyclic voltammogram similar to that reported before,[27-28]

characterized by peaks corresponding to surface oxidation/reduction. The oxidation peak during the positive-going scan is the result of Cu oxide formation ($Cu^0 \rightarrow CuO$), while the reduction peaks are associated with the reverse reaction, being $CuO \rightarrow Cu_2O$ and $Cu_2O \rightarrow Cu^0$, respectively, when scanning from positive to negative.[29-30] Much decreased double layer charging current (-0.2 - 0.2 V vs RHE) and oxidation current (0.5 - 0.8 V vs RHE) are observed on the P4VP-modified Cu electrode, implying that fewer Cu sites are electrochemically accessible due to the presence of P4VP layer.

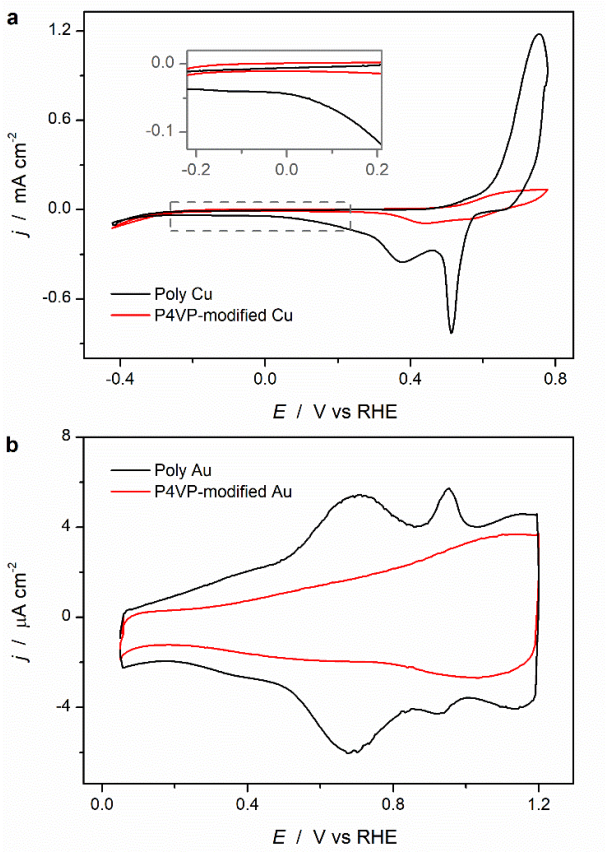

Figure 2.1 The cyclic voltammograms of (a) poly Cu and (b) poly Au with (red) and without (black) a P4VP layer, measured at 50 mV/s in CO_2 saturated 0.1 M $KHCO_3$ solution.

Gold was characterized similarly (Figure 2.1b), where the reversible peaks at 0.7 and 0.95 V vs RHE in this case correspond to the electrochemical lifting of the Au (110) and Au (111) surface reconstructions. Although the peaks associated with the lifting of the surface reconstruction of gold have been associated with sulfate adsorption,[31-32] they were also observed in 0.1 M $KHCO_3$ solutions in a previous work reported by our group.[33] With the

presence of a P4VP layer, these reconstruction-peaks diminish greatly, leaving a broad double layer current, which confirms the decreased permeability of the electrolyte to the reaction interface.

In addition to cyclic voltammetry, AFM was used to characterize the morphology of the electrodes, as depicted in Figure A.1. Figures A.1a, c represent poly Cu and poly Au surfaces respectively, with both electrodes showing typical metallic polycrystalline surfaces with grain boundaries. After modification with P4VP layer, for P4VP-modified Cu (Figure A.1b) and Au electrodes (Figure A.1d), respectively, the morphologies of the surfaces become smoother compared to the uncoated surfaces. This indicates that the P4VP layer fully covers the electrode surfaces, yielding a significant reduction in surface roughness. Additionally, dark spots can be observed in Figures A.1b and d, representing small holes in P4VP film, which confirms previous reports of a P4VP layer adopting a mesoporous structure.[34]

Figure 2.2 depicts the effects on CO_2RR performance after chemical modification of a polycrystalline Cu surface with a P4VP layer. The partial current densities of the dominant products (H_2, CO and HCOOH) are shown in Figure 2.2a, with the dashed and solid lines representing unmodified and P4VP-modified Cu electrodes, respectively. Associated FEs (including observed minority products) are depicted in Figures 2.2b and 2.2c, for the unmodified and P4VP-modified Cu electrodes, respectively. Even though other products (ethanol, n-propanol etc.) have been reported as possible products,[1] they were not detected under our working conditions. The total current density of CO_2RR-related products on P4VP-modified Cu is higher than on unmodified Cu at low overpotentials. This is especially clear at -0.6 V vs RHE, where the combined partial current density of CO_2RR-related products on the P4VP-modified Cu electrode is almost four times higher than on unmodified Cu. Additionally, at this potential, the current density for H_2 production on the P4VP-modified Cu electrode is a factor of three lower. These results demonstrate that the presence of the P4VP layer promotes the reduction of CO_2 and simultaneously suppresses the HER, especially at low overpotentials. Besides enhancing the total activity of the CO_2RR, product selectivity is also changed. FEs for HCOOH, CO and H_2 are 13%, 5% and 87%, respectively,

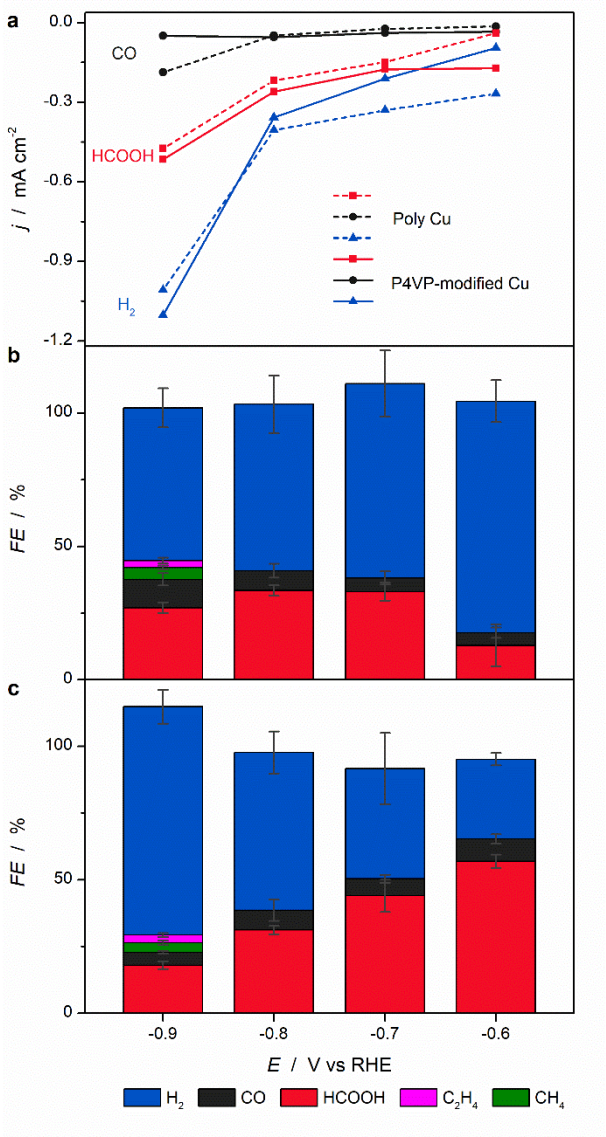

Figure 2.2 CO_2RR performance in CO_2 saturated 0.1 M $KHCO_3$**.** (a) Partial current density of H_2, HCOOH, CO as a function of potential on unmodified Cu (dashed line) and P4VP-modified Cu (solid line), with the FEs for observed products on **(**b) poly Cu and **(**c) P4VP-modified Cu. Error bars are standard deviations based on three measurements.

for unmodified Cu at -0.6 V vs RHE, whilst on P4VP-modified Cu, the FEs are 57%, 8% and 33%, respectively, leading to an enhancement factor of 4.4 for HCOOH and 1.6 for CO. The partial current density and FEs for CO_2RR products (HCOOH and CO) on P4VP-modified Cu remains higher than unmodified electrode at -0.7 V vs RHE. However, at more negative potentials, especially at -0.9 V vs RHE, the partial current density of CO on unmodified Cu electrode increases, while it remains at the same level at less negative potential on P4VP-

modified Cu electrode. Correspondingly, the FEs of CO, CH_4 and C_2H_4 on P4VP-modified Cu are lower than on unmodified Cu electrode. Our data therefore suggests that the P4VP layer enhances HCOOH formation, and increases the selectivity of HCOOH at low overpotentials, while it has a negative effect on the selectivity of CH_4 and C_2H_4 at high overpotentials.

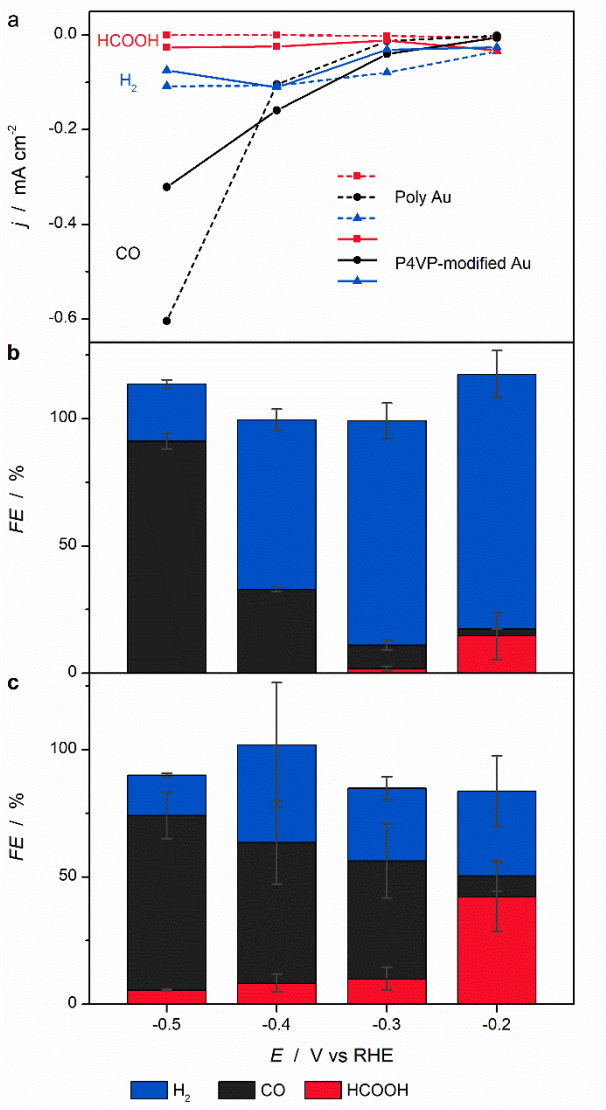

Figure 2.3 CO_2RR performance in CO_2 saturated 0.1 M $KHCO_3$. (a) Partial current density of H_2, HCOOH, CO as a function of potential on poly Au (dashed line) and P4VP-modified Au (solid line), with the FEs for observed products on (b) poly Au and (c) P4VP modified polycrystalline Au shown as bars. Errors bars are standard deviations based on three measurements.

To gain additional insights into the mechanism underlying the observed P4VP effects, we continue to investigate the CO_2RR on unmodified and P4VP-modified poly Au electrodes. Figure 2.3 shows CO_2RR performance of unmodified and P4VP-modified Au electrodes in CO_2 saturated 0.1 M $KHCO_3$. It can be seen in Figures 2.3a (dashed line) and 2.3b that, at low overpotentials, unmodified poly Au predominantly forms hydrogen with only minor amounts of HCOOH and CO, with the former having a relatively higher FE. At increasingly negative potentials, CO_2 reduction gradually takes over, and CO becomes the dominant product whilst HCOOH disappears entirely. In contrast, HCOOH formation is observed on P4VP-modified Au in the entire investigated potential region, as shown in Figure 2.3a (solid line) and Figure 2.3c. Notably, HCOOH is the dominant product at -0.2 V vs RHE with a FE of 42%, although the overall rate is low.

To exclude the possible catalytic effect of the P4VP layer itself, we performed CO_2 reduction on the unmodified pyrolytic graphite and P4VP-modified pyrolytic graphite electrodes (with pyrolytic graphite electrode being chosen for its poor CO_2RR performance). Measured cyclic voltammograms, and the obtained total current densities at -0.6 V vs RHE on the pyrolytic graphite and P4VP-modified pyrolytic graphite electrodes are shown in Figure A.2. No CO_2RR products were detected. Therefore, the P4VP layer itself is catalytically inert. This result confirms that the effect of P4VP layer on the activity and selectivity of the CO_2RR results from the interaction of P4VP layer and metallic active sites (poly Cu and Au).

In an attempt to unravel the origin of the improved CO_2RR performance, we further employed in situ ATR-SEIRAS to study the surface adsorbates, as well as the interfacial electrolyte species. Figure 2.4 shows the in situ ATR-SEIRA spectra recorded on unmodified Cu (Figure 2.4a) and P4VP-modified Cu (Figure 2.4b) during linear sweep voltammetry (LSV) experiment, scanning from +0.3 to -0.9 V vs RHE at a scan rate of 1 mV/s in CO_2-saturated 0.1 M $KHCO_3$, with the background spectra taken at OCP in Milli-Q water. Besides the H_2O bending peak at 1650 cm^{-1},[35-38] various bands related to surface adsorbates and electrolyte species are observed in the ATR-SEIRA spectra, with an overview of the different bands pertinent to this work being provided in Table A.1. It can be seen in Figure 2.4a that,

on a polycrystalline copper surface, the dominant bands in the ATR spectrum at +0.3 V vs RHE are located at 1640 and 1511 cm^{-1}, and can be attributed to a combination of the H_2O bending band (1650 cm^{-1}) and the asymmetrical stretching of HCO_3^- in solution (1620 cm^{-1}) for the former,[36-39] with the latter being indicative of adsorbed CO_3^{2-}.[37, 40-41] Additional minor bands are located at 2343, 2001, 1420 and 1330 cm^{-1}, which correspond to solution phase (dissolved) CO_2,[42] bridge-bound CO ($CO_{ad,bridge}$) and solution-phase CO_3^{2-} and HCO_3^-,[37, 39, 41, 43-44] respectively. When the potential is scanned to more negative potentials, the band associated with adsorbed CO_3^{2-} red-shifts from 1511 cm^{-1} at +0.3 V vs RHE to 1462 cm^{-1} at -0.9 V vs RHE as a result of the Stark tuning effect, with the intensity of this band gradually decreasing as CO_3^{2-} starts to desorb due to the negatively charged interface at more negative potentials.[37, 40-41] The band at 2001 cm^{-1} (related to $CO_{ad,bridge}$) is similarly found to redshift when the potential is scanned to more negative values whilst simultaneously increasing in intensity, whereas the band at 2343 cm^{-1} diminishes due to solution-phase CO_2 being depleted by the CO_2RR at increasingly negative potentials. As for the bands related to solution-phase CO_3^{2-} and HCO_3^-, their intensity is too weak to make meaningful observations and we will therefore not further discuss. Besides these bands, a number of additional bands starts to appear during the negative-going scan. Although $CO_{ad,bridge}$ is visible already at +0.3 V vs RHE, we know from experiments conducted at higher potential that this band starts to increase from -0.1 V vs RHE. Therefore, we believe that $CO_{ad,bridge}$ at the onset of LSV is an artifact from the initial electrochemical preparation of the surface, with the actual onset of this band being at -0.1 V vs RHE. When the potential is scanned further negative, a broad peak at 2050 cm^{-1} starts to appear from -0.5 V vs RHE, ascribed to top-bound CO ($CO_{ad,top}$) on Cu (100) terrace sites.[43] The appearance of this peak is accompanied by the formation of a sharp band at 2070 cm-1, which is assigned to $CO_{ad,top}$ on Cu (100) and (111) step sites.[45-46] The latter band becomes increasingly dominant as the potential is scanned further towards -0.9 V vs RHE. Overall, on poly Cu surface, the adsorbed species as well as solution species are changing as a function of the applied potential, the main adsorbates being $CO_3^{2-}{}_{ad}$ at low overpotential and adsorbed CO at more negative potential.

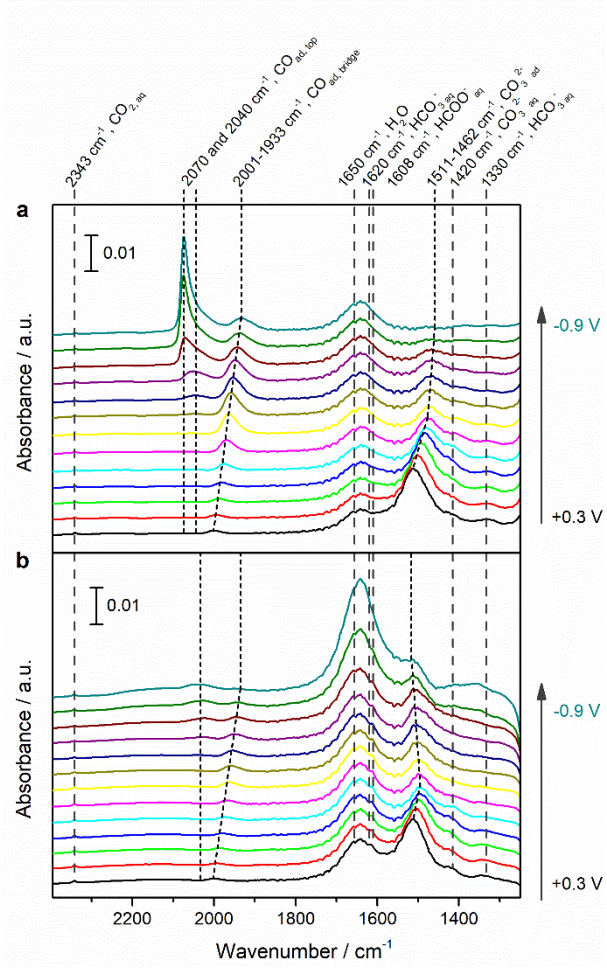

Figure 2.4 ATR-SEIRA spectra of the CO_2RR on (a) poly Cu and (b) P4VP-modified Cu during linear sweep voltammetry at 1 mV/s from 0.2 to -0.9 V vs RHE in CO_2 saturated 0.1 M $KHCO_3$. The background spectrum was taken at OCP in H_2O before experiments. The potential interval between spectra is 0.1 V.

A new working electrode was prepared for ATR-SEIRAS experiments on P4VP-modified Cu. To ensure system integrity and surface reproducibility, the copper surface was characterized with ATR-SEIRAS prior to adding a P4VP layer, although the LSV was halted at -0.5 V vs RHE to ensure stability of the surface. As shown in Figure A.3, the presence of $CO_{ad,top}$ and $CO_{ad,bridge}$ confirms the reproducibility of ATR-SEIRA spectra on the poly Cu surface. The in situ ATR-SEIRA spectra obtained on a P4VP-modified Cu electrode are depicted in Figure 2.4b. Although the P4VP layer seems less stable at the end of LSV (band related to H_2O and HCO_3^- at 1620 cm^{-1} starts to increase at -0.8 and -0.9 V vs RHE), the bands corresponding to

different interfacial species are located at the same positions during the CO_2RR. However, after P4VP modification, an additional band at 1608 cm^{-1} is observed, which is assigned to the asymmetric stretching of solution-phase $HCOO^-$.[37] Contrary to unmodified Cu, at more negative potentials, the band related to $CO_{ad,top}$ on (100)/(111) step sites (2070 cm^{-1}) is barely present on P4VP-modified Cu, while the bands corresponding to adsorbed $CO_{ad,top}$ and $CO_{ad,bridge}$ on (100) terraces (2040 and 2001 cm^{-1}, respectively) exhibit reduced intensity. With higher CO production (see partial current density, Figure 2.2a) on P4VP-modified Cu between -0.6 and -0.8 V vs RHE, these differences in the CO adsorption band indicate fewer active sites on P4VP-modified Cu, which suggests that the P4VP layer coordinates with Cu active sites, especially with step sites. Furthermore, these reduced CO adsorption bands could also explain the lower selectivity of CH_4 and C_2H_4 on P4VP-modified Cu electrode. Overall, the discussed results reveal the effect of P4VP layer on adsorbed CO, suggesting an interaction between P4VP layer and metallic poly Cu surface. However, the ATR-SEIRAS results do not give a clear indication of the effect of P4VP layer on interfacial solution species due to the low band intensity.

In previous literature,[36, 39] ATR-SEIRAS experiments were applied to determine local pH via the ratio of carbon dioxide and bicarbonate vibrational bands on polycrystalline Au electrodes. To gain further insight into the effect of the modification by P4VP on the near-electrode solution-phase species, we performed in situ ATR-SEIRAS on unmodified Au and P4VP-modified Au electrodes. Figures 2.5a and 2.5b show the recorded ATR-SEIRA spectra during LSV at 1 mV/s in CO_2 saturated 0.1 M $KHCO_3$ for unmodified and P4VP-modified Au, respectively. Although adsorbed CO bands were observed around 2000 cm^{-1} on Au electrodes in previous work,[33, 47-48] they were not observed under our working conditions. We observe only bands related to H_2O and solution-phase species; CO_2, HCO_3^-, CO_3^{2-}. Additionally, on P4VP-modified Au, there is a very weak feature at 1608 cm^{-1}, which may be assigned to solution $HCOO^-$.[37] However, the band attributed to electrolyte HCO_3^- has a much lower relative intensity on P4VP-modified Au surface, suggesting different local environments after adding the P4VP layer. Instead of looking at absolute band intensity, the ratio of the integrals of the bands related to dissolved CO_2 and solution HCO_3^- (2343 and 1620 cm^{-1}, respectively;

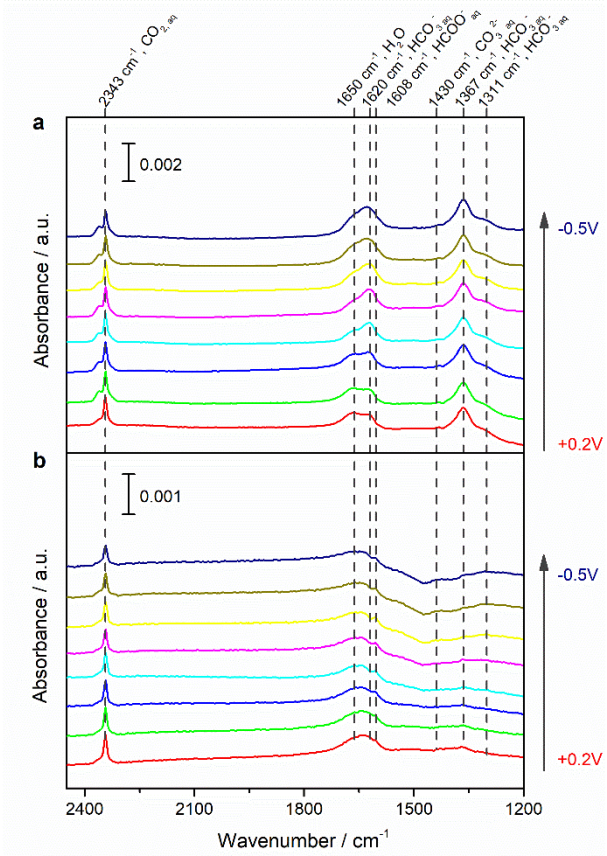

Figure 2.5 ATR-SEIRA spectra of the CO_2RR on (a) poly Au and (b) P4VP-modified Au during linear sweep voltammetry at 1 mV/s from 0.2 to -0.5 V vs RHE in CO_2 saturated 0.1 M $KHCO_3$. The background spectrum was taken at OCP in pure H_2O prior to ATR-SEIRAS experiments. The potential interval between spectra is 0.1 V.

I_{CO2} / I_{HCO3}^-) was calculated as an indicator of local environment. To avoid convolution with the H_2O bending band, I_{CO2} / I_{HCO3}^- was determined from in situ ATR-SEIRA spectra taken in D_2O, as the D_2O bending band is shifted to 1208 cm^{-1}. Figure A.4 shows the ATR-SEIRA spectra, obtained on unmodified Au and P4VP-modified Au electrodes in CO_2 saturated 0.05 M K_2CO_3 in D_2O. The calculated I_{CO2} / I_{HCO3}^- ratio as a function of applied potential for both surfaces is shown in Figure 2.6. On unmodified Au electrodes, the obtained I_{CO2} / I_{HCO3}^- agrees with literature reports.[36, 39] Specifically, in the potential region of 0.3 to -0.1 V vs RHE, where no HER nor CO_2RR occurs, I_{CO2} / I_{HCO3}^- remains constant; when the negative-going scan enters the region of -0.2 to -0.4 V vs RHE, where HER and CO_2RR start, I_{CO2} / I_{HCO3}^- keeps decreasing due to the CO_2 consumption and HCO_3^- formation, as a consequence of the

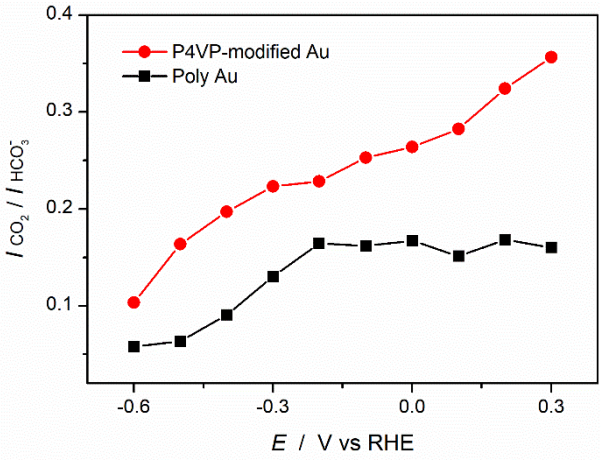

Figure 2.6 Potential dependency of I_{CO2} / I_{HCO3^-} on poly Au (black) and P4VP-modified Au (red), calculated from ATR-SEIRA spectra obtained during LSV at 1 mV/s in CO_2 saturated 0.1M $KDCO_3$ in D_2O. The background spectrum was taken at OCP in D_2O before experiments.

reaction between CO_2 and OH^-; finally, from -0.5 V vs RHE onwards, I_{CO2} / I_{HCO3^-} reaches the lowest point, where CO_2 is almost depleted and HCO_3^- starts to be consumed by the excess OH^-, and as a result, CO_3^{2-} finally become the dominant solution species near the electrode. On the other hand, on the P4VP-modified Au, the obtained I_{CO2} / I_{HCO3^-} (Figure 2.6, red line) is always higher than on the unmodified Au and keeps decreasing with the negative-going scan. The higher value of I_{CO2} / I_{HCO3^-} in the potential region between 0.3 and -0.1 V vs RHE indicates the limited mass transport of HCO_3^- (compared with CO_2) from bulk electrolyte to the P4VP-Cu interface. Moreover, the decreasing I_{CO2} / I_{HCO3^-} in this potential region (where no reaction occurs) suggests slow HCO_3^- diffusion from bulk electrolyte to the P4VP-Cu interface. Therefore, we propose that this water insoluble P4VP layer not only limits the mass transport of H_2O, but also limits the mass transport of HCO_3^-. Both species are proton donor of HER during the CO_2RR, thereby lowering HER activity. As a result, less OH^- formation is expected due to the limited HER, and hence less CO_2 is consumed by homogeneous reaction (with OH^-) during the CO_2RR, which could explain the higher I_{CO2} / I_{HCO3^-} on the P4VP-modified surface at more negative potential. Overall, we show the I_{CO2} / I_{HCO3^-} as an indicator of the local environment, which is the CO_2/HCO_3^- equilibrium resulting

from reactions (both HER and CO_2RR) at the interface as well we the mass transport from the bulk electrolyte to the interface. We have assigned the inhibited HER on P4VP-modified Cu and Au electrodes to the limit transport of H_2O and HCO_3^-, however, the CO_2RR products distribution is still depends on the nature of the catalysts and the applied potential. Therefore, it is not possible to directly correlate I_{CO2} / I_{HCO3^-} ratios with CO or HCOOH yield.

As a final consideration, we investigated surface hydrophobicity, as an indicator of surface and H_2O interaction, via contact angle measurements. Figure A.5 shows the contact angles between a water droplet and our investigated surfaces. Unmodified Au shows the most hydrophobic surface with a contact angle of 91 degrees. Upon modification with a P4VP layer, both Cu and Au electrodes shows the same contact angle (57 degrees), which is more hydrophilic than poly Au. Surprisingly, unmodified poly Cu exhibits the most hydrophilic surface (17 degrees), which is probably due to the presence of a CuOx layer when the copper surface is exposed to air. However, CV preparation employed in this work prior to the CO_2RR experiments is expected to remove this CuOx layer, and therefore, a more hydrophobic surface of metallic poly Cu is expected under CO_2RR conditions. Overall, the contact angle measurements show different interaction between H_2O and the employed working electrodes. It has been suggested previously that hydrophilic additives improve HCOOH selectivity during the CO_2RR, by influencing the formation of surface hydrides.[24]

2.4 Conclusions

In this work, we investigated the effect of chemical modification via the addition of a P4VP layer on CO_2RR of poly Cu and Au electrodes. We have shown that the presence of P4VP layer hinders the HER while it enhances the CO_2RR, especially HCOOH formation, on both electrodes. Less CO-adsorption bands on P4VP-modified Cu and higher I_{CO2} / I_{HCO3^-} ratios on P4VP-modified Au are observed from in situ ATR-SEIRAS experiments, compared to unmodified electrodes. This indicates inhibited mass transport of H_2O and HCO_3^- from the bulk to the catalytically active sites with the presence of a P4VP layer, whilst also suggesting coordination between the P4VP layer and Cu sites. In addition, contact angle measurement shows P4VP modification influences the hydrophilicity of the surface, which influences

surface hydride formation,[24] resulting in enhanced and preferential HCOOH formation at low overpotential (with respect to CO). We believe that this is an important experimental finding highlighting that the electrolyte side of the catalyst is very important in steering selectivity, so much so that even a catalyst such as Au can produce substantial amounts of HCOOH. Our work offers further understanding of enhanced the CO_2RR activity and selectivity on P4VP layer modified electrodes, and confirms that functionalization by tailored additives is a promising strategy for developing selective catalysts.

References

1. Kuhl, K. P.; Cave, E. R.; Abram, D. N.; Jaramillo, T. F., New insights into the electrochemical reduction of carbon dioxide on metallic copper surfaces. *Energy Environ. Sci.* **2012,** *5* (5), 7050-7059.
2. Hatsukade, T.; Kuhl, K. P.; Cave, E. R.; Abram, D. N.; Jaramillo, T. F., Insights into the electrocatalytic reduction of CO_2 on metallic silver surfaces. *Phys. Chem. Chem. Phys.* **2014,** *16* (27), 13814-9.
3. Montoya, J. H.; Shi, C.; Chan, K.; Norskov, J. K., Theoretical Insights into a CO Dimerization Mechanism in CO_2 Electroreduction. *J. Phys. Chem. Lett.* **2015,** *6* (11), 2032-7.
4. Hanselman, S.; Koper, M. T. M.; Calle-Vallejo, F., Computational Comparison of Late Transition Metal (100) Surfaces for the Electrocatalytic Reduction of CO to C_2 Species. *ACS Energy Lett.* **2018,** *3* (5), 1062-1067.
5. Kortlever, R.; Shen, J.; Schouten, K. J.; Calle-Vallejo, F.; Koper, M. T., Catalysts and Reaction Pathways for the Electrochemical Reduction of Carbon Dioxide. *J. Phys. Chem. Lett.* **2015,** *6* (20), 4073-4082.
6. Durst, J.; Rudnev, A.; Dutta, A.; Fu, Y.; Herranz, J.; Kaliginedi, V.; Kuzume, A.; Permyakova, A. A.; Paratcha, Y.; Broekmann, P.; Schmidt, T. J., Electrochemical CO_2 Reduction - A Critical View on Fundamentals, Materials and Applications. *Chimia (Aarau)* **2015,** *69* (12), 769-776.
7. Oloman, C.; Li, H., Electrochemical processing of carbon dioxide. *ChemSusChem* **2008,** *1* (5), 385-91.
8. Yang, Z. N.; Oropeza, F. E.; Zhang, K. H. L., P-block metal-based (Sn, In, Bi, Pb) electrocatalysts for selective reduction of CO_2 to formate. *Apl Materials* **2020,** *8* (6).
9. Min, X.; Kanan, M. W., Pd-catalyzed electrohydrogenation of carbon dioxide to formate: high mass activity at low overpotential and identification of the deactivation pathway. *J. Am. Chem. Soc.* **2015,** *137* (14), 4701-8.
10. Gao, D.; Zhou, H.; Wang, J.; Miao, S.; Yang, F.; Wang, G.; Wang, J.; Bao, X., Size-dependent electrocatalytic reduction of CO_2 over Pd nanoparticles. *J. Am. Chem. Soc.* **2015,** *137* (13), 4288-91.
11. Dinh, C. T.; Burdyny, T.; Kibria, M. G.; Seifitokaldani, A.; Gabardo, C. M.; Garcia de Arquer, F. P.; Kiani, A.; Edwards, J. P.; De Luna, P.; Bushuyev, O. S.; Zou, C.; Quintero-Bermudez, R.; Pang, Y.; Sinton, D.; Sargent, E. H., CO_2 electroreduction to ethylene via hydroxide-mediated copper catalysis at an abrupt interface. *Science* **2018,** *360* (6390), 783-787.
12. Chen, X.; Chen, J.; Alghoraibi, N. M.; Henckel, D. A.; Zhang, R.; Nwabara, U. O.; Madsen, K. E.; Kenis, P. J. A.; Zimmerman, S. C.; Gewirth, A. A., Electrochemical CO_2-to-ethylene conversion on polyamine-incorporated Cu electrodes. *Nat. Catal.* **2020,** *4* (1), 20-27.
13. Wang, X.; Klingan, K.; Klingenhof, M.; Moller, T.; Ferreira de Araujo, J.; Martens, I.; Bagger, A.; Jiang, S.; Rossmeisl, J.; Dau, H.; Strasser, P., Morphology and mechanism of highly selective Cu(II) oxide nanosheet catalysts for carbon dioxide electroreduction. *Nat. Commun.* **2021,** *12* (1), 1-12.
14. Pavesi, D.; Dattila, F.; Van de Poll, R. C. J.; Anastasiadou, D.; García-Muelas, R.; Figueiredo, M.; Gruter, G.-J. M.; López, N.; Koper, M. T. M.; Schouten, K. J. P., Modulation of the selectivity of CO_2 to CO electroreduction in palladium rich Palladium-Indium nanoparticles. *J. Catal.* **2021,** *402*, 229-237.
15. Ponnurangam, S.; Yun, C. M.; Chernyshova, I. V., Robust Electroreduction of CO_2 at a Poly(4-vinylpyridine)-Copper Electrode. *ChemElectroChem* **2016,** *3* (1), 74-82.

16. Han, Z.; Kortlever, R.; Chen, H. Y.; Peters, J. C.; Agapie, T., CO_2 Reduction Selective for $C_{\geq 2}$ Products on Polycrystalline Copper with N-Substituted Pyridinium Additives. *ACS Cent. Sci.* **2017,** *3* (8), 853-859.
17. Ahn, S.; Klyukin, K.; Wakeham, R. J.; Rudd, J. A.; Lewis, A. R.; Alexander, S.; Carla, F.; Alexandrov, V.; Andreoli, E., Poly-Amide Modified Copper Foam Electrodes for Enhanced Electrochemical Reduction of Carbon Dioxide. *ACS Catal.* **2018,** *8* (5), 4132-4142.
18. Thevenon, A.; Rosas-Hernandez, A.; Peters, J. C.; Agapie, T., In-Situ Nanostructuring and Stabilization of Polycrystalline Copper by an Organic Salt Additive Promotes Electrocatalytic CO_2 Reduction to Ethylene. *Angew. Chem. Int. Ed. Engl.* **2019,** *58* (47), 16952-16958.
19. Wei, X.; Yin, Z.; Lyu, K.; Li, Z.; Gong, J.; Wang, G.; Xiao, L.; Lu, J.; Zhuang, L., Highly Selective Reduction of CO_2 to C_{2+} Hydrocarbons at Copper/Polyaniline Interfaces. *ACS Catal.* **2020,** *10* (7), 4103-4111.
20. Wagner, A.; Sahm, C. D.; Reisner, E., Towards molecular understanding of local chemical environment effects in electro- and photocatalytic CO_2 reduction. *Nat. Catal.* **2020,** *3* (10), 775-786.
21. Sharifi Golru, S.; Biddinger, E. J., Effect of additives in aqueous electrolytes on CO_2 electroreduction. *Chem. Eng. J.* **2021,** *428*, 131303-131323.
22. Mu, S.; Li, L.; Zhao, R.; Lu, H.; Dong, H.; Cui, C., Molecular-Scale Insights into Electrochemical Reduction of CO_2 on Hydrophobically Modified Cu Surfaces. *ACS Appl. Mater. Interfaces* **2021,** *13* (40), 47619-47628.
23. Gutierrez-Sanchez, O.; Daems, N.; Bulut, M.; Pant, D.; Breugelmans, T., Effects of Benzyl-Functionalized Cationic Surfactants on the Inhibition of the Hydrogen Evolution Reaction in CO_2 Reduction Systems. *ACS Appl. Mater. Interfaces* **2021,** *13* (47), 56205-56216.
24. Buckley, A. K.; Lee, M.; Cheng, T.; Kazantsev, R. V.; Larson, D. M.; Goddard, W. A., III; Toste, F. D.; Toma, F. M., Electrocatalysis at Organic-Metal Interfaces: Identification of Structure-Reactivity Relationships for CO_2 Reduction at Modified Cu Surfaces. *J. Am. Chem. Soc.* **2019,** *141* (18), 7355-7364.
25. Cave, E. R.; Montoya, J. H.; Kuhl, K. P.; Abram, D. N.; Hatsukade, T.; Shi, C.; Hahn, C.; Norskov, J. K.; Jaramillo, T. F., Electrochemical CO_2 reduction on Au surfaces: mechanistic aspects regarding the formation of major and minor products. *Phys. Chem. Chem. Phys.* **2017,** *19* (24), 15856-15863.
26. Monteiro, M. C. O.; Philips, M. F.; Schouten, K. J. P.; Koper, M. T. M., Efficiency and selectivity of CO_2 reduction to CO on gold gas diffusion electrodes in acidic media. *Nat. Commun.* **2021,** *12* (1), 1-7.
27. Ren, D.; Wong, N. T.; Handoko, A. D.; Huang, Y.; Yeo, B. S., Mechanistic Insights into the Enhanced Activity and Stability of Agglomerated Cu Nanocrystals for the Electrochemical Reduction of Carbon Dioxide to n-Propanol. *J. Phys. Chem. Lett.* **2016,** *7* (1), 20-4.
28. Klingan, K.; Kottakkat, T.; Jovanov, Z. P.; Jiang, S.; Pasquini, C.; Scholten, F.; Kubella, P.; Bergmann, A.; Roldan Cuenya, B.; Roth, C.; Dau, H., Reactivity Determinants in Electrodeposited Cu Foams for Electrochemical CO_2 Reduction. *ChemSusChem* **2018,** *11* (19), 3449-3459.
29. Tang, W.; Peterson, A. A.; Varela, A. S.; Jovanov, Z. P.; Bech, L.; Durand, W. J.; Dahl, S.; Norskov, J. K.; Chorkendorff, I., The importance of surface morphology in controlling the selectivity of polycrystalline copper for CO_2 electroreduction. *Phys. Chem. Chem. Phys.* **2012,** *14* (1), 76-81.
30. Simon, G. H.; Kley, C. S.; Roldan Cuenya, B., Potential-Dependent Morphology of Copper Catalysts During CO_2 Electroreduction Revealed by In Situ Atomic Force Microscopy. *Angew. Chem.*

Int. Ed. Engl. **2021,** *60* (5), 2561-2568.
31. Hamelin, A., Cyclic voltammetry at gold single-crystal surfaces. Part 1. Behaviour at low-index faces. *J. Electroanal. Chem.* **1996,** *407* (1-2), 1-11.
32. Yoshida, K.; Kuzume, A.; Broekmann, P.; Pobelov, I. V.; Wandlowski, T., Reconstruction and electrochemical oxidation of Au(110) surface in 0.1 M H_2SO_4. *Electrochim. Acta* **2014,** *139*, 281-288.
33. Marcandalli, G.; Villalba, M.; Koper, M. T. M., The Importance of Acid-Base Equilibria in Bicarbonate Electrolytes for CO_2 Electrochemical Reduction and CO Reoxidation Studied on Au(hkl) Electrodes. *Langmuir* **2021,** *37* (18), 5707-5716.
34. Tapan, N. A., CO_2 electroreduction on P4VP modified copper deposited gas diffusion layer electrode: pH effect. *Mater. Renew. Sustain. Energy* **2016,** *5* (4), 1-10.
35. Shaw, S. K.; Berna, A.; Feliu, J. M.; Nichols, R. J.; Jacob, T.; Schiffrin, D. J., Role of axially coordinated surface sites for electrochemically controlled carbon monoxide adsorption on single crystal copper electrodes. *Phys. Chem. Chem. Phys.* **2011,** *13* (12), 5242-51.
36. Ayemoba, O.; Cuesta, A., Spectroscopic Evidence of Size-Dependent Buffering of Interfacial pH by Cation Hydrolysis during CO_2 Electroreduction. *ACS Appl. Mater. Interfaces* **2017,** *9* (33), 27377-27382.
37. Moradzaman, M.; Mul, G., Infrared Analysis of Interfacial Phenomena during Electrochemical Reduction of CO_2 over Polycrystalline Copper Electrodes. *ACS Catal.* **2020,** *10* (15), 8049-8057.
38. Larsen, O. F.; Woutersen, S., Vibrational relaxation of the H_2O bending mode in liquid water. *J. Chem. Phys.* **2004,** *121* (24), 12143-5.
39. Dunwell, M.; Yang, X.; Setzler, B. P.; Anibal, J.; Yan, Y.; Xu, B., Examination of Near-Electrode Concentration Gradients and Kinetic Impacts on the Electrochemical Reduction of CO_2 using Surface-Enhanced Infrared Spectroscopy. *ACS Catal.* **2018,** *8* (5), 3999-4008.
40. Sartin, M. M.; Yu, Z.; Chen, W.; He, F.; Sun, Z.; Chen, Y.-X.; Huang, W., Effect of Particle Shape and Electrolyte Cation on CO Adsorption to Copper Oxide Nanoparticle Electrocatalysts. *J. Phys. Chem. C* **2018,** *122* (46), 26489-26498.
41. Arihara, K.; Kitamura, F.; Ohsaka, T.; Tokuda, K., Characterization of the adsorption state of carbonate ions at the Au(111) electrode surface using in situ IRAS. *J. Electroanal. Chem.* **2001,** *510*, 128-135.
42. Falk, M.; Miller, A. G., Infrared spectrum of carbon dioxide in aqueous solution. *Vib. Spectrosc* **1992,** *4*, 105-108.
43. Hori, Y.; Koga, O.; Watanabe, Y.; Matsuo, T., FTIR measurements of charge displacement adsorption of CO, on poly- and single crystal (100) of Cu electrodes. *Electrochim. Acta* **1998,** *44* (8-9), 1389-1395.
44. Gunathunge, C. M.; Ovalle, V. J.; Li, Y.; Janik, M. J.; Waegele, M. M., Existence of an Electrochemically Inert CO Population on Cu Electrodes in Alkaline pH. *ACS Catal.* **2018,** *8* (8), 7507-7516.
45. Koga, O.; Teruya, S.; Matsuda, K.; Minami, M.; Hoshi, N.; Hori, Y., Infrared spectroscopic and voltammetric study of adsorbed CO on stepped surfaces of copper monocrystalline electrodes. *Electrochim. Acta* **2005,** *50* (12), 2475-2485.
46. Gunathunge, C. M.; Li, X.; Li, J.; Hicks, R. P.; Ovalle, V. J.; Waegele, M. M., Spectroscopic Observation of Reversible Surface Reconstruction of Copper Electrodes under CO_2 Reduction. *J. Phys. Chem. C* **2017,** *121* (22), 12337-12344.
47. Rodriguez, P.; Garcia-Araez, N.; Koverga, A.; Frank, S.; Koper, M. T., CO electroxidation on

gold in alkaline media: a combined electrochemical, spectroscopic, and DFT study. *Langmuir* **2010,** *26* (14), 12425-32.

48. Wuttig, A.; Yaguchi, M.; Motobayashi, K.; Osawa, M.; Surendranath, Y., Inhibited proton transfer enhances Au-catalyzed CO_2-to-fuels selectivity. *Proc. Natl. Acad. Sci. U.S.A.* **2016,** *113* (32), E4585-93.